Journal of Materials Chemistry B

Accepted Manuscript

This is an *Accepted Manuscript*, which has been through the Royal Society of Chemistry peer review process and has been accepted for publication.

Accepted Manuscripts are published online shortly after acceptance, before technical editing, formatting and proof reading. Using this free service, authors can make their results available to the community, in citable form, before we publish the edited article. We will replace this *Accepted Manuscript* with the edited and formatted *Advance Article* as soon as it is available.

You can find more information about *Accepted Manuscripts* in the Information for Authors.

Please note that technical editing may introduce minor changes to the text and/or graphics, which may alter content. The journal's standard Terms & Conditions and the Ethical guidelines still apply. In no event shall the Royal Society of Chemistry be held responsible for any errors or omissions in this *Accepted Manuscript* or any consequences arising from the use of any information it contains.

ROYAL SOCIETY OF CHEMISTRY

www.rsc.org/materialsB

rGO Quantum Dots/ZnO Hybrid Nanofibers Fabricated Using Electrospun Polymer Templates and Applications in Drug Screen Involved in Intracellular H_2O_2 Sensor

Chi Yang[a],*, Ling-wei Hu [b], Hong-Yan Zhu[a], Yong Ling[a], Jin-Hua Tao[a], Chun-Xiang Xu[c],**

[a] Department of Pharmacy, Nantong University, Nantong 226001, China

[b] Shangqiu Medical College, Shangqiu 476100, Henan, China

[c]State Key Laboratory of Bioelectronics, Southeast University, Nanjing 210096, China

*Corresponding authors.Tel.: +86-513-85051728, E-mail: toyangchi@ntu.edu.cn.
**Corresponding authors. Tel.: +86-25-83790755, E-mail: xcxseu@seu.edu.cn.

KEYWORDS reduced graphene oxide quantum dots; ZnO; hydrogen peroxide; intracellular sensor; drug screen

ABSTRACT: Through years, the reported intracellular H_2O_2 sensors just focused on the unrelated measurements of the intracellular H_2O_2 generated from the stimulus of Cd^{2+}, ascorbic acid (AA) etc., leading to difficulty in data interpretation. Here, a novel reduced graphene oxide quantum dots(rGO QDs)/ZnO hybrid nanofibers-based electrochemical biosensor for the detection of intracellular H_2O_2 released from cancer and normal cells under the stimuli of the corresponding anticancer drugs permits a quantitative study of the interaction between the target drug compound and the cancer cell, which is suitable for candidate drug screening. Nylon 6/6 nanofibers are used as robust templates for the facile fabrication of novel rGO QDs/ZnO hybrid nanofibers via an electrospinning followed by a step hydrothermal growth method. The as-made sensor was applied to determine the H_2O_2 released from prostate cancer cell (PC-3) versus noncancerous cell (BPH-1) under the stimuli of the corresponding anticancer drugs (apigenin, antisense CK2α etc). The amount of the H_2O_2 released from the PC-3 cancer cell is about (320±12) amol $cell^{-1}$ and about (210±6) amol $cell^{-1}$ for the BPH-1 noncancerous cell under the stimuli of specific therapy drug antisense CK2α. These results demonstrate that rGO QDs/ZnO hybrid nanofibers-based electrochemical biosensor can efficiently detect the distinct amounts of H_2O_2 released from cancer and noncancer cells.

INTRODUCTION

Recently, ZnO nanofibers (ZnO NFs) have attracted extensive interests in different research fields because of their excellent properties, repeatable and controllable fabrication process.[1] Most notably, ZnO nanofibers-based sensors possess high sensitivities, low limits of detection, fast electron transfer kinetics, and they have been widely used for the detection of molecules, such as glucose, CO, ethanol, etc.[2-4] The analytical performances of these sensors depend on the electrochemical activity and biocompatibility of ZnO NFs, which are strongly affected by their surface hybrid components. Several strategies, including electrospinning technology, hydrothermal route, and spray pyrolysis method of hybridization, have been developed for fabricating the hybrid ZnO NFs to impart desirable properties, such as enhanced sensing capabilities and catalytic performance. For instance, the hybridization of phosphotungstic acid (PWA) and ZnO NFs through electrospinning technology leads to excellent electrocatalytic activity toward the oxidation of dopamine at a low potential.[5] And some metal or metal oxide particles can either decorate the surface of the ZnO NFs or be encapsulated within the interior of the ZnO NFs to enhance catalytical activity.[6,7] Besides these attractive features, hybridizing graphene sheets with ZnO NFs to yield a large number of friction sites onto the ZnO surfaces is proven to be an efficient method to regulate the structural and electronic properties of the ZnO NFs. In principle, the zero dimensional nanomaterials of

Journal of Materials Chemistry B Accepted Manuscript

graphene oxide quantum dots(rGO QDs) with more superior performance should be more favorable for sensing. Considering these interesting properties, we employ polymer nanofibers as templates to fabricate novel hybrid nanofibers of rGO QDs/ZnO via an electrospinning technique and hydrothermal process by one step and investigate the sensing performance of the resulted sample towards hydrogen peroxide (H_2O_2).

As is distributed in most of the mammalian cells,[8] H_2O_2 participates in the signal transduction processes in a concentration dependent manner.[9] At low concentrations, it serves as a second messenger in cellular signal transduction and plays an important role in protecting the living body.[10-12] Whereas at a high concentration, it can damage major cellular constituents and harm to living organisms, causing a number of pathological events ranging from aging, neurodegeneration, to cancer.[13-16] Therefore, the quantitative determination of intracellular H_2O_2 is of great value in elaborating its regulation of signal transduction pathways and searching for new therapeutic strategies for cancer and other diseases. Recently, enzyme-based electrochemical biosensors for the quantitative detection of intracellular H_2O_2 have received considerable attention due to their great advantages include high sensitivity and selectivity, rapid response, easy miniaturization and good quantitative ability.[17-20] The main shortcoming is that enzymes would not maintain their activity under the detection conditions because of their intrinsic nature. Whereas, those which were capable of measuring H_2O_2 with extremely high stability used nanomaterials including precious metal nanoparticles,[21,22] carbon nanomaterials,[23,24] and metal compound nanostructures,[25,26] which would solve the problems of the low long-term operational stability. However, so far the reported intracellular H_2O_2 sensors just focused on the unrelated measurements of the intracellular H_2O_2 generated from the stimulus of Cd^{2+}, ascorbic acid (AA) etc. which were added in the detection system by researchers, leading to difficulty in data interpretation. Thus, it is necessary and reasonable to explore a quantitative detection of the intracellular H_2O_2 released from cancer and normal cells under the straightforward stimuli of the corresponding anticancer drugs permitting a quantitative study of the interaction between the target drug compound and the cancer cell, which may be suitable for candidate drug screening.

Herein, the novel hybrid nanofibers of rGO QDs/ZnO with random or quasi-aligned were prepared using polymer nanofibers as templates *via* an electrospinning technique and hydrothermal process by one step. The experimental procedure is shown in Scheme 1. The obtained hybrid nanofibers exhibit high electrocatalytic activity towards H_2O_2 and achieve highly sensitive detection of H_2O_2 at the nanomolar level, which are ascribed to their large surface area as well as their synergistic effect. Moreover, the as-made sensor can also be used for monitor intracellular H_2O_2 by quantitative electrochemical measurements. By studying the effects of the stimulator loading (anticancer drug), distinct H_2O_2 generation is site-detected in cancer cells as compared to the normal ones. Therefore, comparing to the tedium of animal models of drug screening, this work has demonstrated a simple and effective sensing platform for detection of dynamic release of H_2O_2 from cells, which has potential utility to drug screen.

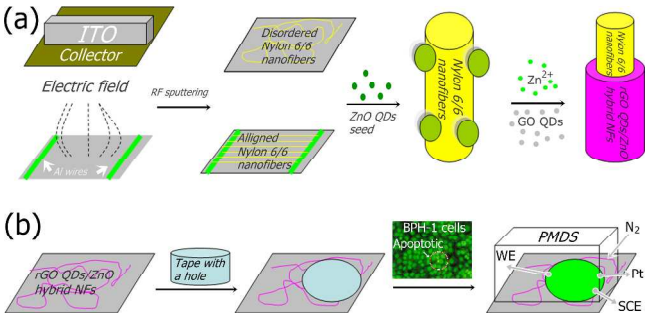

Scheme 1. (a) Illustration of the synthetic route of rGO QDs/ZnO hybrid nanofibers and (b) fabrication of the cell-based intracellular H_2O_2 Sensors.

RESULTS AND DISCUSSION

Electrospinning is a simple and convenient method for fabricating 1D nanomaterials, especially for nanofibers, which is easy in geometric control, diverse in composition, and has a low cost.[27] The terminal diameter of the whipping jet is therefore controlled by the flow rate, the electric current, and the surface tension of the complex fluid. Recently, Sigmund et al.[28] gave the relations between the nanofiber diameter and the process-governing variables as below:

$$\bar{\varepsilon}\pi\gamma = 2\pi d^3\left(\frac{I-\pi EKd^2}{2Q}\right)\times\left(2\ln\left(\frac{c}{d^3\sqrt{I-\pi EKd^2}}\right)-3\right) \quad (1)$$

where $\bar{\varepsilon}$ is the dielectric permittivity of air, γ as the surface tension, Q as liquid

Journal of Materials Chemistry B Accepted Manuscript

jet flow rate, *I* as the total current directed toward the lower electrode, *K* as the electric conductivity, *c* as a constant and *d* as the jet diameter. Based on the above theory, the terminal jet radius *d* can be adjusted by the corresponding parameters. In addition, the aligned fibers could be controlled by applied the electrical field during the electrospinning processes.[29]

By comprehensively considering the parameters mentioned before, we fixed the nylon 6/6 concentration at 20 wt. % and the applied voltage at 15 kV accordingly (other data not shown in the paper). Figure 1(a) reveals the SEM images of electrospun nylon 6/6 nanofibers with average diameters of 168 nm. The electrospun nanofibers have uniform diameters, smooth surfaces, and are randomly oriented on the indium tin oxide (ITO) glass slides. The density of the nanofiber networks can be controlled by varying the electrospinning duration. In order to align the fibers in parallel to each other along some axis, two stripes of aluminum wires were placed along opposite edges of the substrate and connected to the ground terminal of the power supply that applied the electrical field between the jet and the substrate during the electrospinning processes. This imposed a directional distribution of the electrical field flux lines between the jet and the aluminum wires, as depicted in Figure 1a, facilitating alignment of segments of the fibers across the aluminum wires.[30] The difference between the nonaligned and quasi-aligned nylon 6/6 fibers is clearly observed in the scanning electron microscopy (SEM) micrographs in Figure 1a (left and right graphs, respectively).

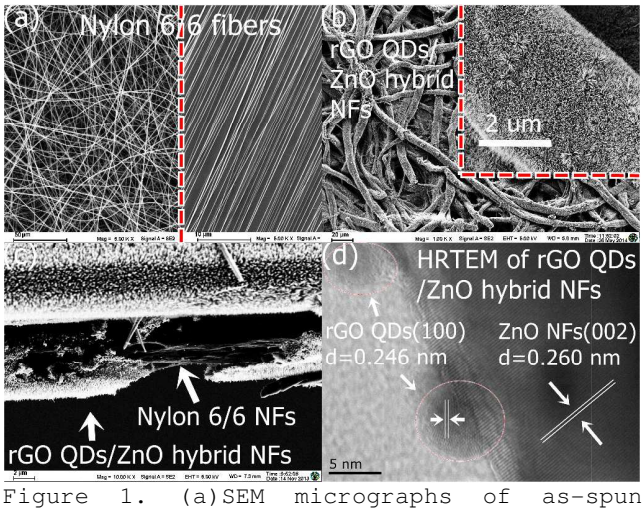

Figure 1. (a)SEM micrographs of as-spun Nylon 6/6 fibers (left, nonaligned; right, quasi-aligned); (b) the rGO QDs/ZnO hybrid NFs (insert with the high magnification); (c) tilted view image of a broken part of a Nylon 6/6 fiber coated with rGO QDs/ZnO hybrid composite overlayer; (d)high resolution of rGO QDs/ZnO hybrid NFs.

Following the electrospinning process nylon 6/6 nanofibers were coated with ZnO nanoparticles as seeds (Figure S1) by a dip-coating technique.[22] Subsequently, the nylon 6/6 nanofibers covered with ZnO seeds were immersed into a aqueous solution of an equimolar mixture of zinc acetate dihydrate ($Zn(CH_3COO)_2 \cdot 2H_2O$, 0.025 M), hexamethylene tetramine($C_6H_{12}N_4$, 0.025 M) and graphene oxide quantum dots(GO QDs, ~1 mg/mL, an optimum amount of content,[31] see Figure S2). The hydrothermal process was conducted at 90 °C for 6 h. After this reaction, rGO QDs/ZnO hybrid nanostructures were grown successfully on the electrospun nylon 6/6 nanofibers that penetrate the fiber network and cover the entire length of the nanofibers (Figure 1b). On the basis of the previous works by others,[32] a possible mechanism for the formation of rGO QDs/ hybrid NFs may contain the following process. Firstly, due to the electrostatic attraction, the GO QDs were adsorbed on the surface of ZnO seeds. Meanwhile, a part of Zn^{2+} ions were adsorbed on the surface of GO to form coagulation. Then, the Zn^{2+} ions were converted first to $Zn(OH)_4^{2-}$ and then to ZnO (Eqs 2, 3). During the process, the GO QDs were also reduced to rGO QDs.

$$Zn^{2+} + 4OH^- \longrightarrow Zn(OH)_4^{2-} \quad (2)$$

$$Zn(OH)_4^{2-} \longrightarrow ZnO + H_2O + 2OH^- \quad (3)$$

The diameter of the rGO QDs/ZnO hybrid NFs is about 800 nm (Figure 1b), much larger than the diameter of nylon 6/6 nanofibers (168 nm) due to the attachment of rGO QDs/ZnO hybrid nanostructures. From the high-magnification image (Figure 1b, inserted), it can be seen that the nylon 6/6 nanofibers were capped with brush-like nanostructures uniformly. For our amazing, SEM images showed that the nylon 6/6 fibers template was not scratched off and removed during the proposed hydrothermal process (Figure 1c). Lattice images obtained at even higher magnifications displayed lattice fringes that can be identified with crystallographic planes of the ZnO and rGO QDs structure.[33] For instance, lattice fringes having interplanar spacing of ~0.246 nm and ~0.26 nm, corresponding to rGO QDs (100) planes and ZnO (002), respectively, are highlighted in the Figure 1d. The high-resolution TEM (HRTEM) image also suggests

Journal of Materials Chemistry B Accepted Manuscript

that rGO QDs did not enwrap ZnO nanofibers completely.

X-ray diffraction (XRD) pattern obtained from electrospun rGO QDs/ZnO hybrid NFs is presented in Figure 2a. Bragg peaks corresponding to ZnO and rGO QDs are observed simultaneously, indicating that the rGO QDs/ZnO hybrid NFs have been successfully synthesized from GO QDs and zinc acetate dihydrate powder. The existence of the rGO QDs on the ZnO nanostructure is confirmed by the exhibition of a broad intense G (002) diffraction peak at 2θ=26.1 °. The XRD analysis further showed that the main diffraction peaks of rGO QDs/ZnO composite were similar to that of pure ZnO and corresponded to wurtzite-structured ZnO (JPCDS 36-1451), which indicated that the presence of graphene did not result in the development of new crystal orientations or changes in preferential orientations of ZnO. No typical diffraction peaks of carbon species were observed, which was attributed to the low amount of graphene in the composite.[34]

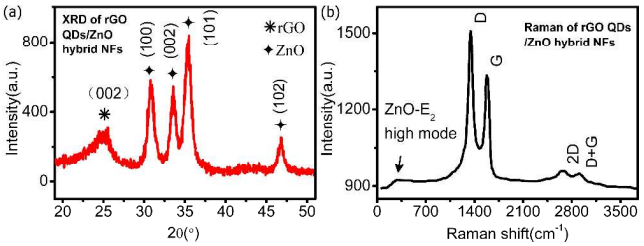

Figure 2. (a)XRD patterns of rGO QDs/ZnO hybrid NFs; (b) Raman spectra of rGO QDs/ZnO hybrid NFs.

The major Raman features as seen from the Raman spectra of these rGO QDs/ZnO hybrid NFs in Figure 2b are the D band at around 1345 cm^{-1} as a breathing mode of k-point phonons of A1g symmetry, which is assigned to the local defects and disorder, especially at the edges of graphene, and the G band at around 1591 cm^{-1}, which is usually assigned to the E2g phonon of C sp^2 atoms.[35,36] However, the intensity ratio of the D and G bands (I_D/I_G) of the hybrids was much higher than that of oxide graphene (see Figure S2b), attributed to interactions between the ZnO nanostructure and the reduced oxide graphene.[37] The hybrid fibers also shows the $2E_2$(M) mode of ZnO at 326 cm^{-1}.[38] Moreover, in agreement with the earlier literature the Raman spectrum of rGO QDs shows two new bands, 2D band at 2762 cm^{-1} and the D + G band at 2933 cm^{-1}, showing the graphitization the carbon framework.[39,40]

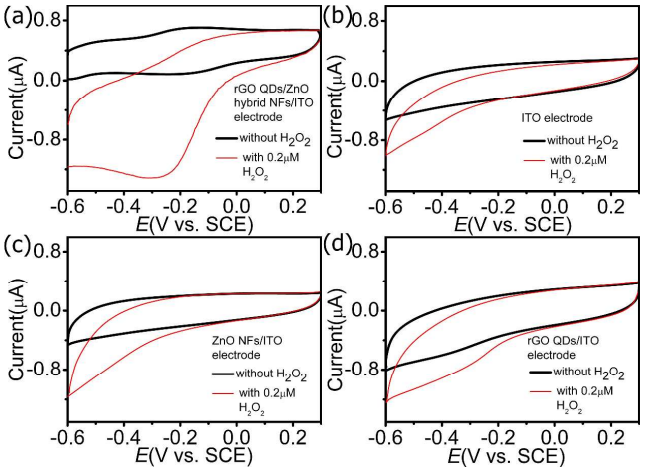

Figure 3. Voltammetric responses of the rGO QDs/ZnO hybrid NFs/ITO (a), ITO (b), ZnO NFs/ITO (c), and rGO QDs/ITO electrodes (d) in N_2-saturated PBS (0.1 M, pH 7.2) with (red curve) and without (black curve) 0.2 μM H_2O_2. Scan rate was 100 mV s^{-1}.

We evaluated the electrocatalytic activity of the rGO QDs/ZnO hybrid NFs (in our experiments, we select the nonaligned fibers) modified ITO electrode toward reduction of H_2O_2 in 0.1 M PBS (pH = 7.2) with the protection of N_2. Figure 3 shows the cyclic voltammetric (CV) of the (a) rGO QDs/ZnO hybrid NFs/ITO, (b) ITO, (c) ZnO NFs/ITO, and (d) rGO QDs/ITO electrodes in the absence (black line) and presence of 0.2 μM (red line) H_2O_2 in the N_2-saturated 0.1 M PBS solution (pH 7.2). In the absence of H_2O_2, no reduction peaks were observed at (b) bare ITO, (c) ZnO NFs /ITO, and (d) rGO QDs/ITO electrode. Similarly, in the presence of H_2O_2, there is no obvious reduction peaks generated on (b) bare ITO, and (c) ZnO NFs /ITO electrodes, except only a weak reduction peak of H_2O_2 at −0.28 V was observed on the (d) rGO QDs/ITO electrode. In contrast, (a) rGO QDs/ZnO hybrid NFs/ITO displayed a pair of small oxidative and reductive peak in the potential range of −0.6 ~ 0.3 V in the absence of H_2O_2 and a remarkable reduction peak in the presence of H_2O_2 from −0.6 to 0.3 V. These results suggest that the rGO QDs/ZnO hybrid NFs electrode possesses efficient electrocatalytic activity toward the reduction of H_2O_2, which provides an approach for detecting H_2O_2 at the low reduction potential. Chronoamperometry could be used for the evaluation of the catalytic rate constant (index of electrocatalytic activity) with the help of the following equation: [41]

$$\frac{I_C}{I_L}=\lambda^{0.5}[\pi^{0.5}erf(\lambda^{0.5})+\frac{\exp(-\lambda)}{\lambda^{0.5}}] \qquad (4)$$

Journal of Materials Chemistry B Accepted Manuscript

where I_C and I_L are the currents in the presence and absence of H_2O_2, respectively, $\lambda = K_{cat}C_t$ is the argument of the error function, K_{cat} is the catalytic rate constant, and t is elapsed time. In the case where $\lambda > 1.5$, erf ($\lambda^{1/2}$) is almost equal to unity, the above equation can be reduced to:

$$\frac{I_C}{I_L} = \lambda^{0.5}\pi^{0.5} = (K_{cat}C_t)^{0.5}\pi^{0.5} \quad (5)$$

From the slope of the plot: I_C/I_L versus $t^{1/2}$, as shown in Figure 4a, the mean value of K_{cat} for H_2O_2 oxidation was calculated to be 2.1×10^7 cm^3 mol^{-1} s^{-1}. This value is higher than that obtained at graphene/poly(3,4-ethylenedioxythiophene) /iron hexacyanoferrate electrode (4.0×10^6 cm^3 mol^{-1} s^{-1}) [42]but less than that obtained at cubic nickel hexacyanoferrate /polyaniline/carbon nanotubes/platinum electrode (1.29×10^8 cm^3 mol^{-1} s^{-1}). [43] The results showed the catalytic rate of H_2O_2 on rGO QDs/ZnO hybrid NFs electrode is fast.[44]

The high electrocatalytic activity of rGO QDs/ZnO composite may arise from the following aspects. Firstly, the study of the adsorption of a H_2O_2 molecule on the ZnO and O-vacancy defected ZnO showed that the zinc atoms of the defect are more reactive toward H_2O_2 reduction to H_2O.[45] During the adsorption process, the H_2O_2 was reoriented in such a way that its O atom has diffused into vacancy site, so that O/O and O/H bonds of the molecule were dissociated and an H_2O is formed. Thus, we think that ZnO may be a candidate for electrochemical reduction of H_2O_2 and inferred the following reaction:

$$Oi^-/Oi^{2-} + H_2O_2 \longrightarrow O_2(g) + H_2O + e^-/2e^- \quad (6)$$

Secondly, it can be attributed to the high density of edge-plane-like defective sites on graphene, which might provide many active sites for electron transfer and reduced the H_2O_2 (Eqs.7).[46-49]

$$rGO\text{-}(C\text{-}OH)n + H_2O_2 \longrightarrow O_2(g) + H_2O + rGO \quad (7)$$

The structures of ZnO graphene-like[50] made it easy for the form of rGO QDs/ZnO hybrid composite, which leading synergistic effect of the rGO QDs and ZnO. Other plausible reason for the enhanced catalytic activity can be ascribed to the oxygen-containing groups in ZnO nanofibers providing large amounts of anchoring sites for the deposition of rGO QDs during the synthesis of the rGO QDs/ZnO composite and control the rGO QDs without aggregation. The well-dispersed rGO QDs on the surface of ZnO renders more accessible surfaces of rGO QDs over the bulk ones for the H_2O_2 reduction, leading to their higher electrochemical activity.

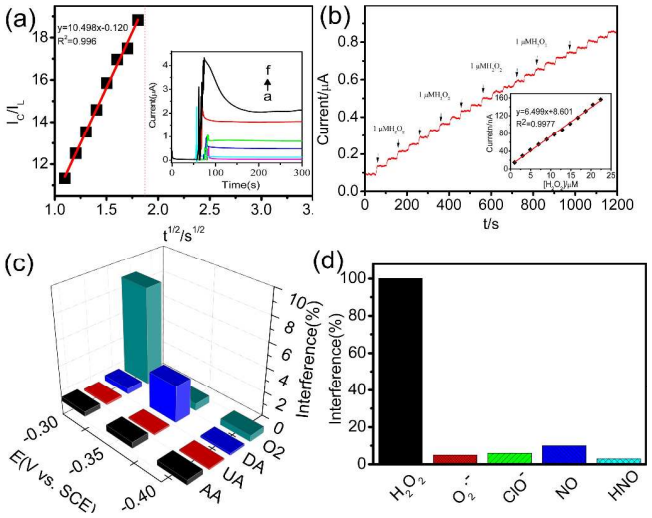

Figure 4. (a) Chronoamperograms obtained at the rGO QDs/ZnO hybrid NFs/ITO in the (a) absence and presence of (b) 5, (c) 70, (d) 120, (e) 250, and (f) 350 nM of H_2O_2, first and second potential steps were −0.6 and −0.3 V vs. SCE, respectively. Left: dependence of I_C/I_L on $t^{1/2}$ derived from the data of chronoamperogams of (a) and (f) in the main panel. (b) Amperometric i-t response at rGO QDs/ZnO hybrid NFs upon successive additions of 1-22 μM H_2O_2 into continuously stirred N_2 saturated 0.1 M PBS (pH 7.2). Applied potential: −0.4 V. Inset (below) is the plot of response current vs. $[H_2O_2]$. (c) The typical selectivity profile of the present biosensor obtained at different applied potentials: −0.3, −0.35, −0.4 V versus SCE (derived from the data of Figure S3. (d) ROS selectivity obtained at −0.4 V versus SCE.

Figure 4b shows the typical steady state amperometric response of the rGO QDs/ZnO hybrid NFs electrode with the successive addition of H_2O_2 into the stirred N_2 saturated 0.1 M PBS at −0.4 V(from the CV electrocatalysis and selectivity test). After the addition of H_2O_2, this sensor could achieve the steady-state current within 3 s, which indicated fast response time. The corresponding calibration curve for the H_2O_2 sensor is shown in the inset of Figure 4b. The response displays a good linear range from 1 to 22.48 μM with a correlation coefficient of 0.997 and a slope of (6.49+0.15) μA μM^{-1}. Therefore, the sensitivity is calculated to be 101.46 $\mu A \mu M^{-1}$ cm^{-2} (see inset of Figure 4b). The detection limit is estimated to be ca. (0.025±0.001) μM (at a signal/noise of 3), which is much lower than those reported

Journal of Materials Chemistry B Accepted Manuscript

previously.[22] These analytical parameters are compared with other reported H_2O_2 sensors (Table 1). These results indicate that the rGO QDs/ZnO hybrid NFs electrode is a good platform for the detection of H_2O_2 and can be used to detect the physiological levels of H_2O_2. Therefore, the tests of reproducibility and storage stability are very important. The relative standard derivation (RSD) of its current response for the addition of 0.2 μM H_2O_2 was 5.5 % for 8 successive measurements, which suggested good precision (see Figure S3a). The electrode-to-electrode reproducibility was also estimated from the response to 0.2 μM H_2O_2 at six different electrodes. The RSD of 5.8 % was obtained, indicating acceptable fabrication reproducibility (data not shown). In order to investigate the stability of the sensor, the current response to 0.2 μM of H_2O_2 was monitored periodically. The results demonstrated that the variation of the response current at the rGO QDs/ZnO hybrid NFs electrode decreased to about 95 % of its initial response current on the fifth day (see Figure S3b), indicating the excellent stability of the sensor. The loss of the response current may ascribe to the adsorption of species on the surface of the electrode.[51] Adsorption of the species could block contact of the rGO QDs/ZnO hybrid NFs electrode surface with H_2O_2 and the electron transfer between the electrode and solution, decreasing the reduction of H_2O_2.

Meanwhile, the selectivity of the rGO QDs/ZnO hybrid NFs for the detection of H_2O_2 was also evaluated. Figure 4c shows most commonly existing interference under different applied potentials. At the negative potential, e.g. −0.3 V, the present H_2O_2 biosensor was free from anodic interferences like 1 mM ascorbic acid (AA), 1 mM uric acid (UA), 1 mM dopamine (DA), and 1 mM glucose, but 8 % of cathodic response current from 4 μM O_2 was observed relative to 2 μM H_2O_2. On the other hand, at the more negative potential, e.g. −0.35 V, 3 % of anodic current of 1 mM DA was obtained relative to 2 μM H_2O_2, indicating that the AA interferes with the response of the sensor to H_2O_2. Fortunately, at this lower potential of −0.4 V, the oxidation of DA did not occur at rGO QDs/ZnO hybrid NFs. Importantly, the reduction peak currents of H_2O_2 had no change in the presence and absence of O_2. Therefore, for fulfilling both the selectivity and sensitivity of the present biosensor, low-potential was selected as the working potential. In addition, the selectivity of the present H_2O_2 over reactive oxygen species (ROS) was also examined. As demonstrated in Figure 4d, negligible interferences were observed for other typical ROS including $O_2^{\bullet-}$, ClO^-, NO, HNO. These results convincingly indicated that the present rGO QDs/ZnO hybrid NFs electrode showed high selectivity for typical ROS, O_2, and other biological species at the low-potential detection.

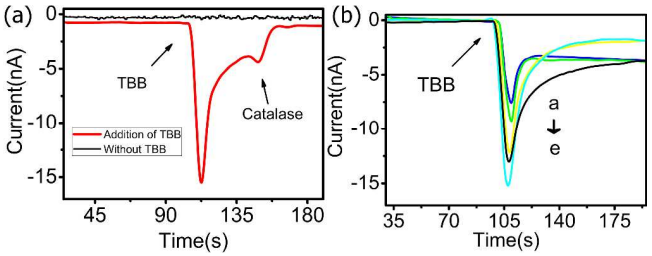

Figure 5. (a) Amperometric responses of the rGO QDs/ZnO hybrid NFs/ITO electrode for the reduction of H_2O_2 released from BPH-1 cells without (a) and with (b) the addition of 0.2 μM TBB. (b) The time course of H_2O_2 released from the BPH-1 cells induced by (a) 0.5, (b) 0.4, (c) 0.1, (d) 0.3, and (e) 0.2 μM TBB.

The proposed sensor was applied to perform real-time detection of endogenous generation of H_2O_2 in the BPH-1 cells induced by 4,5,6,7-tetrabromobenzotriazole (TBB). Without the stimulation of TBB, BPH-1 cells did not generate any measurable signal at the electrode under the applied potential of −0.4 V (Figure 5a). When 0.2 μM TBB was introduced into the solution, the current increased sharply to a peak value, indicative of the release of H_2O_2 from the cells after being treated with TBB. After a stable response is reached, injecting 300 UmL^{-1} catalase, a selective scavenger of H_2O_2, into the solution, the response of H_2O_2 at the electrode disappears (Figure 5a) since the releasing H_2O_2 was scavenged by catalase, demonstrating that the addition of TBB may induce the release of H_2O_2 from the BPH-1 cells and cannot lead to the release of other ROS or RNS. In the control experiment, upon the addition of TBB in the cell-free detection solution, no obvious signal was observed (Figure S5), further suggesting that H_2O_2 was generated from cells by the stimulation of TBB. A maximum current of ca.15 nA is obtained at ca. 23 s after injection of TBB. This current corresponds to the H_2O_2 amount of (10.45±0.1) nmol, which was calculated based on the calibration curve depicted in inset of Figure 4b. Therefore, the mean flux of H_2O_2 releasing from the cells is evaluated to be (690±7) amol $cell^{-1}$. These results suggest that the developed biosensor could be useful in determination of cellular H_2O_2. The cells were exposed

Journal of Materials Chemistry B Accepted Manuscript

to TBB at concentrations ranging from 0.1 to 0.5 mM was studied (Figure 5b). The corresponding flux of H_2O_2 as shown in Figure 6a, the amount of H_2O_2 in BPH-1 cell is significantly increased with the enhancement of the TBB concentration, and it reaches the highest value (ca. 691±8 amol $cell^{-1}$) at an TBB concentration of 0.2 μM, after that, the concentration of H_2O_2 generated by the cells decreases with the enhancement of the TBB loading. This may be because an extra high concentration of H_2O_2 induced by the high loading of TBB can damage the lipid membrane of the cells and even cause cell death (the image of the cells on the ITO surface is depicted in Scheme 1b).[52] And this result leads to the decrease in the amount of released H_2O_2. Therefore, a concentration of 0.2 μM for TBB is applied in subsequent treatment of cells. In addition, the amount of H_2O_2 generated in BPH-1 cells is also affected by the time of TBB treatment. Figure 6b depicts the time course experimental results with TBB loading at a constant concentration of 0.2 μM for TBB. The value of H_2O_2 in BPH-1 cells is significantly increased after treatment with 0.2 μM TBB. The concentration of H_2O_2 increases with the increase of the inducement time and the highest value is attained at the time of 60 min. Afterwards the concentration decreases gradually and reaches a relatively stable value (ca. 518±10 amol $cell^{-1}$) at 5 h. These results demonstrate that low concentration of H_2O_2 in living cells can indeed be successfully detected by the developed electrode, which represents a new biosensing platform for a reliable collection of kinetic information of cellular H_2O_2 release and could be potentially useful for oxidative stress biosensors in study of downstream biological effects of various stimuli in physiology and pathology.

As we know, relatively specific chemical drug apigenin and TBB, much more specific biological agent, CK2α (casein kinase 2α) are the anticancer drugs for therapy against prostate cancer. Here, we selected apigenin, TBB, and antisense CK2α as the stimuli and three kinds of cells (Prostatic cancer PC-3 cells, nontumorigenic prostate BPH-1 cells, and noncancerous cell line Chinese hamster ovary (CHO) as model cells. The developed electrode can be also used for measuring the flux of H_2O_2 releasing from the cells induced by a variety of stimuli such as apigenin, TBB, and antisense CK2α, which were reported to induce the generation of H_2O_2 in cells. The amount of H_2O_2 generated in the cells and the flux of H_2O_2 from the cells are significantly dependent on the stimuli. PC-3 cells, BPH-1 cells, and CHO cells were equally responsive to treatment with apigenin or TBB as indicated by the intracellular H_2O_2 production. However, treatment of these cells with antisense CK2α oligonucleotide showed a distinctly differential response in cancer versus noncancer cells, such that although the H_2O_2 production was comparable in cancer (PC-3) and noncancer (BPH-1 and CHO) cells in response to apigenin or TBB it was minimal in noncancer cells treated with antisense CK2α oligonucleotide (Figure 6c). This could be ascribed to antisense CK2α oligonucleotide as more effective in down-regulation of CK2α and result in induction of intracellular H_2O_2.[53-55] These results demonstrated that the antisense CK2α is more specific to prostate cancer, which agreement with the reported results.[56]

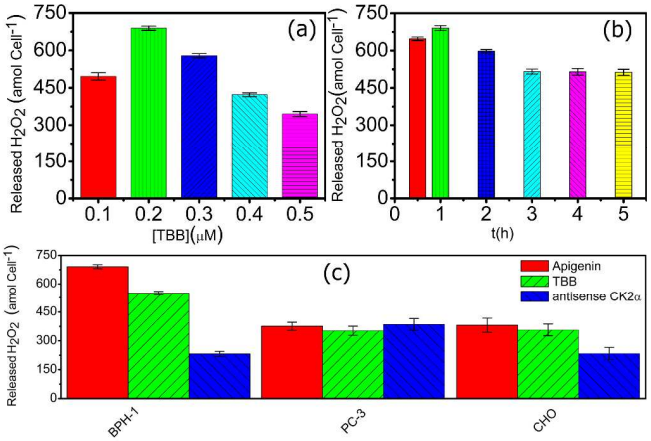

Figure 6. (a) Dependence of the amount of H_2O_2 generated in BPH-1 cells on the concentration of TBB at a fixed treatment time of 60 min, and on the treatment time at a fixed TBB concentration of 0.2 μM. (b) Comparison of intracellular H_2O_2 production in prostatic cancer and nontumorigenic cells in response to therapy drug.

CONCLUSIONS

In summary, rGO QDs/ZnO hybrid NFs were synthesized by the combination of a simple electrospinning and thermal treatment processes. The rGO QDs are well dispersed on the surface of ZnO nanofibers. Such rGO QDs/ZnO hybrid NFs exhibited high electroactive surface area, and high electrocatalytic activity toward the reduction of H_2O_2. The fabricated sensor based on rGO QDs/ZnO hybrid NFs with high sensitivity and selectivity against other ROS, oxygen, and other biological species, as well as broad linear range and low detection limit with satisfactory stability and repeatability. Accordingly, the present biosensor has been

Journal of Materials Chemistry B Accepted Manuscript

successfully applied in determination of H_2O_2 released from living cells. Meanwhile, the proposed sensor was evaluated for the H_2O_2 released from prostate cancer cells and noncancerous cells under the stimuli of the corresponding anticancer drugs and the results demonstrated that the sensor could be applied in drug screen. In this way, the proposed device is a promising tool for further drug studies dealing with living cells.

EXPERIMENTAL SECTION

Indium tin oxide (ITO)-coated glass plates with a square resistance of ~ 10 Ωcm^{-2} were purchased from Nanbo Display Technology Co. Ltd. (Shenzhen, China). 4,5,6,7-tetrabromobenzotriazole (TBB) and uric acid (UA) were purchased from Alfa Aesar. Apigenin, dopamine (DA) and catalase were obtained from Sigma-Aldrich. Ascorbic acid (AA, ≥ 99.0 %), 30 % hydrogen peroxide (H_2O_2) and glucose were obtained from Aladdin Chemistry Co. Ltd. catalase (E.C. 1.11.1.6, from bovine liver, lyophilized powder, 2000-5000 U mg^{-1}, Sigma). PC-3 was maintained in RPMI 1640 (Sigma-Aldrich) supplemented with 7 % fetal bovine serum (FBS) and 2 mmol/L L-glutamine and grown in standard T-75 flasks. Chinese hamster ovary (CHO) cell line was purchased from Sigma-Aldrich and maintained in Ham's F12 supplemented with 2 mM Glutamine and 10 % FBS. BPH-1 cell line (benign prostate epithelial cells, Shanghai Gene Core Bio. Technologies Co., Ltd) was maintained in Dulbecco's Modified Eagle's Medium (DME H-21 4.5 g/L glucose) supplemented with 10 % FBS. The sequence for the antisense CK2α oligonucleotide employed in the experiments was 5'-CCTGCTTGGCACGGGTCCCGA CAT-3', which was obtained from Shanghai Gene Core Bio. Technologies Co., Ltd. All the reagents were analytical grade and used as received. All the aqueous solutions were prepared with Milli-Q water (18.2 MΩ cm^{-1}). Except the interference test of O_2 (under O_2 saturated solution), all the experiments were deaerated with high purity nitrogen before experiments. Solutions of H_2O_2 were freshly diluted from the 30 % solution, and their concentrations were determined using a standard $KMnO_4$ solution. All electrochemical experiments were carried out at room temperature.

In the selectivity test, superoxide anion ($O_2^{\bullet-}$) was derived from dissolved KO_2 (10 μM) in the DMSO solution. Hypochlorite anion (ClO^-) was provided by NaClO (10 μM).[48] Nitric oxide (NO) and nitroxyl (HNO) were derived from the solution of S-nitroso-N-acetyl-DL-penicillamine (10 μM) and Angeli's salt (10 μM), respectively.[57,58]

Commercial nylon 6/6 (Mw ~ 262.35 g/mol, Sigma Aldrich) was used as the polymer in the present study. Formic acid and acetic acid were used as-received. 20-wt % nylon 6/6 was dissolved in 4:1 formic acid/acetic acid solvents. This solution was stirred for 3 h at room temperature and loaded into a 10 mL plastic syringe fitted with metallic needles of 0.5 mm of inner diameter. Then the syringes were fixed horizontally on the syringe pump (model SP 101IZ, WPI). The solution was continuously fed through the nozzle using a syringe pump (model SP 101IZ, WPI) at a rate of 0.5 mL/h. High voltage (15 kV) was applied between the needle and the grounded collector 18 cm below it. As a result, a continuous stream was ejected from the nozzle as a long fiber and collected on the substrates. ITO glass slides (1cm×1cm) were used as substrates in specimens for microstructural characterizations and used for biosensing measurements. To obtain uniaxial alignment of the fibers, two stripes of aluminum wires (diameter=0.5 mm) were placed right next to the ITO edges as shown in Figure 1b. The distribution of the electrical field flux lines between the needle and the aluminum wires led to uniaxial alignment of the electrospun fibers perpendicular to the wires. The electrospinning processes were carried out at 25 °C and 30 % relative humidity in an enclosed box. After vacuum dried for 24 h, the fibers were used for further analysis.

The electrospun nanofibers (collected on the ITO) were first dip-coated with the ZnO seed solution (0.1 M, see support information) for 10 min, rinsed with ethanol, heat treated at 90 °C for 1 h, and then dried in air for 24 h. rGO QDs/ZnO hybrid NFs were grown on nylon 6/6 nanofibers using hydrothermal treatment of as-prepared electrospun nylon 6/6. Prepared aqueous solutions of zinc acetate dihydrate ($Zn(CH_3COO)_2 \cdot 2H_2O$, 0.025 M), hexamethylene tetramine ($C_6H_{12}N_4$, 0.025 M) were mixed and stirring for 0.5 h and reduced graphene oxide quantum dots (1mg/mL, see support information). As-prepared electrospun mats (2cm×2cm) with this mixture was then taken into a Teflon crucible and kept inside the autoclave. This autoclave was kept at 90 °C for 5 h. The obtained mat after cooling was washed several times with distilled water and dried in air. By similar procedures, the rGO QDs/ITO and ZnO NFs/ITO were also fabricated, and their electrocatalytic characteristics were compared with those of the rGO QDs/ZnO hybrid NFs/ITO.

Journal of Materials Chemistry B Accepted Manuscript

The fabrication process is schematically shown in Scheme 1b. A piece of punched adhesive tape with a hole (diameter: 4 mm) was attached onto ITO substrate surface, which modified by the rGO QDs/ZnO hybrid NFs and prepared as the working electrode. Then H_2O_2 suspension in pH 7.2 PBS with the volume of 8 μL was dropped on the hole. Followed by a piece of filter paper with 6 mm long and 6 mm wide was covered on the hole. After that a calomel electrode (SCE) wire and a Pt wire were integrated with the ITO glass (working electrode, WE) to form the electrochemical detection system. And last the three electrode detection device was integrated in a PDMS cover.

The release flux of H_2O_2 from cells was measured with the use of the rGO QDs/ZnO hybrid NFs electrode. Typically, Prostate cancer cells BPH-1 were maintained in RPMI-1640 supplemented with 10 % FBS and incubated at 37 °C in a humidified incubator (5 % CO_2 - 95 % air). At the logarithmic growth phase, the cells were then washed three times with PBS (0.1 M, pH 7.2) and the cell number was estimated (1.5×10^4 cell mL^{-1}), and 80 μL PBS (0.1 M, pH 7.2) was added for the electrochemical experiments. Before measurements, the buffer was deoxygenated by gently shaking the cells under a humidified nitrogen stream. After a steady state background was attained, 20 μL TBB (0.2 μM) was injected into buffer and response current corresponding to the electrocatalytic reduction of H_2O_2 releasing from the cells was recorded under the physiological pH and temperature (pH 7.2 and 37 °C). The effects of TBB concentration on the release of H_2O_2 from the cells were also evaluated. Various concentrations of TBB (ranging from 0.1 to 0.5 μM) were injected into the buffer to induce the generation of H_2O_2 in the cells, and the flux of H_2O_2 from the cells was measured using the developed electrode. For control experiments, 0.2 μM TBB was added into a PBS buffer without BPH-1 cells. To study the stimulus type-dependent characteristics of the H_2O_2 releasing from the BPH-1 cells, Antisense CK2α, and apigenin was added into the buffer, respectively, with each concentration of 0.2 μM. The release process and the release flux of H_2O_2 were monitored by recording the change of the reduction current of H_2O_2 at the electrode with time. Similarly, PC-3 or CHO (1.5×10^4 cells) were treated with Antisense CK2α, apigenin or TBB (0.2 μM) and monitored by amperometric measurements.

The morphology, uniformity and microstructure evolution of the fibers were investigated after each processing step by using scanning electron microscope (FE-SEM, S-7400, Hitachi, Japan). Transmission electron microscope (TEM, JEOL JEM 2010) was used for the detailed morphological investigation of the rGO QDs/ZnO hybrid NFs. X-ray diffraction (XRD) data of rGO QDs/ZnO hybrid NFs were collected within the range of 2θ=10-55 ° by using Rigaku D/max-2500 Diffractometer with Cu Kα radiation, operating at a voltage of 45 kV and a current of 40 mA. Raman scattering of the hybrid nanostructures were collected on a Ranishaw inVia Raman microscope with an excitation laser of 514 nm. Additionally, all the voltammetric and amperometric measurements were carried out with CHI 660E (Chenhua Shanghai) electrochemical analyzer. Cell apoptosis was measured by acidine orange (100□g/mL)/ethidium bromide (100□g/mL) staining and examined with confocal laser scanning fluorescence microscopy (Nikon 300, USA).

AUTHOR INFORMATION

Corresponding Author

*E-mail: toyangchi@ntu.edu.cn

**E-mail: xcxseu@seu.edu.cn

Present Addresses

[a] Department of Pharmacy, Nantong University, Nantong 226001, China
[b] Shangqiu Medical College, Shangqiu 476100, Henan, China
[c] State Key Laboratory of Bioelectronics, Southeast University, Nanjing 210096, China

Author Contributions

All authors have given approval to the final version of the manuscript.

ACKNOWLEDGMENT

This work was supported by NSFC (Grants 61404075, 81302628, 81102743, 81202467, and 61475035) and (Nos. BK20130394), A Project Funded by the Priority Academic Program Development of Jiangsu Higher Education Institutions, NSFC (Grant 81102327) and the Open Research Fund of State Key Laboratory of Bioelectronics, Southeast University.

REFERENCES

(1) Stafiniak, A.; Boratynski, B.; Baranowska-Korczyc, A.; Fronc, K.; Elbaum, D.; Tłaczała, M. J. Am. Ceram. Soc. **2014**, *97*, 1157-1163.

Journal of Materials Chemistry B Accepted Manuscript

(2) Ahmad, M.; Pan, C. f.; Luo, Z. X.; Zhu, J. J. Phys. Chem. C. **2010**, *114*, 9308–9313.

(3) Katoch, A.; Sun, G. J.; Choi, S. W.; Byun, J. H.; Kim, S. S. Sens. Actuators B. **2013**, *185*, 411–416.

(4) Zhang, Z. Y.; Li, X. H.; Wang, C. H.; Wei, L. M.; Liu, Y. C.; Shao, C. L. J. Phys. Chem. C **2009**, *113*, 19397–19403.

(5) Wu, J. P.; Yin, F. Sens. Actuators B **2013**, *185*, 651–657.

(6) Choi, S. W.; Katoch, A.; Sun, G. J.; Kim, S. S. Sens. Actuators B **2013**, *181*, 787–794.

(7) Wang, C. Y.; Ma, S. Y.; Sun, A. M; Qin, R.; Yang, F. C.; Li, X. B.; Li, F. M.; Yang, X. H. Sens. Actuators B **2014**, *193*, 326–333.

(8) Amatore, C.; Arbault, S.; Guille, M.; Lemaitre, F. Chem. Rev. **2008**, *108*, 2585–2621.

(9) Finkel, T., FEBS Lett. **2000**, *476*, 52–54.

(10) Rhee, S. G. Science **2006**, *312*, 1882–1883.

(11) Finkel, T. Curr. Opin. Cell Biol. **2003**, *15*, 247–254.

(12) Stone, J. R.; Yang, S. Antioxid. Redox Sign. **2006**, *8*, 243–270.

(13) Dröge, W.; Schipper, H.M. Aging Cell, **2007**. *6*, 361–370.

(14) DiMauro, S.; Schon, E. A. Annu. Rev. Neurosci. **2008**, *31*, 91–123.

(15) Finkel, T.; Serrano, M.; Blasco, M. A. Nature **2007**, *448*, 767–774.

(16) Rossi, D. J.; Jamieson, C. H. M.; Weissman, I. L. Cell **2008**, *132*, 681–696.

(17) Zhou, J.; Liao, C.A.; Zhang, L. M.; Wang, Q. G.; Tian, Y. Anal. Chem. **2014**, *86*, 4395–4401.

(18) Kim, S. H.; Kim, B.; Yadavalli, V. K.; Pishko, M. V. Anal. Chem. **2005**, 77, 6828–6833.

(19) Luo, Y. P.; Liu, H. Q.; Rui, Q.; Tian, Y. Anal. Chem. **2009**, *81*, 3035–3041.

(20) Wu, P.; Cai, Z. W.; Chen, J.; Zhang, H.; Cai, C. X. Biosen. Bioelectron. **2011**, *26*, 4012–4017.

(21) Wen, Z. H.; Ci, S. Q.; Li, J. H. J. Phys. Chem. B **2009**, *113*, 13482–13487.

(22) Yu, C. M.; Zhu, Z. K.; Wang, Q. H.; Gu, W.; Bao, N.; Gu, H. Y. Chem. Commun. **2014**, *50*, 7329–7331.

(23) Chang, H. C.; Wang, X. M.; Shiu, K. K.; Zhu, Y. L.; Wang, J. L.; Li, Q. W.; Chen, B. A.; Jiang, H. Biosen. Bioelectron. **2013**, *41*, 789–794.

(24) Xi, F. N.; Zhao, D. J.; Wang, X. W.; Chen, P. Electrochem. Comm. **2013**, *26*, 81–84.

(25) Bai, J.; Jiang, X.; Anal. Chem. **2013**, *85*, 8095–8101.

(26) Wang, T. Y.; Zhu, H. C.; Zhuo, J. Q.; Zhu, Z.W.; Papakonstantinou, P.; Lubarsky, G.; Lin, J.; Li, M. X. Anal. Chem. **2013**, *85*, 10289–10295.

(27) Dzenis, Y. Science **2004**,*304*, 1917–1919.

(28) Sigmund, W.; Yuh, J.; Park, H.; Maneeratana, V.; Pyrgiotakis, G.; Daga, A.; Taylor, J.; Nino, J. C. J. Am. Ceram. Soc. **2006**, *89*, 395–407.

(29) Choi, S. H.; Ankonina, G.; Youn, D. Y.; GeunOh, S.; Hong, J. M.; Rothschild, A.; Kim, I. D. ACS Nano **2009**, *3*, 2623–2631.

(30) Li, D.; Wang, Y.; Xia, Y. Nano Lett. **2003**, *3*, 1167–1171.

(31) Anand, K.; Singh, O.; Singh, M. P.; Kaur, J.; Singh, R. C. Sens. Actuators B. **2014**, *195*, 409–415.

(32) Dey, R. S.; RetnaRaj, C. A. RSC Adv. **2013**, *3*, 25858–25864.

(33) Yin, Z. Y.; Wu, S. X.; Zhou, X. Z.; Huang, X.; Zhang, Q. C.; Boey, F.; Zhang, H. Small **2010**, *6*, 307–312.

(34) Son, D. I.; Kwon, B. W.; Kim, H. H.; Angadi, D. H. B.; Choi, W.K. Carbon **2013**, *59*, 289–295.

(35) Wu, Z. S.; Ren, W. C.; Gao, L. B.; Zhao, J. P.; Chen, Z. P.; Liu, B. L.; Tang, D. M.; Yu, B.; Jiang, C. B.; Cheng, H. M. ACS Nano **2009**, *3*, 411–417.

(36) Ferreira, E. H. M.; Moutinho, M. V. O.; Stavale, F.; Lucchese, M. M.; Capaz, R. B.; Achete, C. A.; Jorio, A. Phys. Rev. B **2010**, *82*, 125429–125437.

(37) Fu, D. Y.; Han, G. Y.; Chang, Y. Z.; Dong, J. H. Mater. Chem. Phys. **2012**, *132*, 673–681.

(38) Pan, D. Y.; Zhang, J. C.; Li, Z.; Wu, M. H. Adv. Mater. **2010**, *22*, 734–738.

(39) Moon, I. K.; Lee, J.; Ruoff, R. S.; Lee, H. Nat. Commun. **2010**, *1*, 73–78.

(40) Wang, H.; Robinson, J. T.; Li, X.; Dai, H. J. Am. Chem. Soc. **2009**, *131*, 9910–9911.

Journal of Materials Chemistry B Accepted Manuscript

(41) Bard, A.J.; Faulkner, L. R.; John Wiley & Sons, Inc., New York, **2001**, pp. 471 (Ch. 12).

(42)José,G.M.C.J.; Grasyelle,M.M. F.; Fernanda,G.O.;Flavio,S.D.; Rita de,C.S.L.J. Electroanal. Chem. **2014**, *732*,93-100.

(43) Wang, Z.D.; Sun, S.B.; Hao, X.G.; Ma, X.L.; Guan, G.Q.; Zhang, Z.L.;Liu ,S.B.Sens. Actuator B-Chem. **2012**, *171-172*, 1073-1080.

(44) Ojani, R.; Raoof, J. B.; Salmany-Afagh, P. J. Electroanal. Chem. **2004**, *571*, 1-8.

(45) Wang, J.; Xu, M.; Zhao, R.; Chen, G. A. Analyst **2010**, *135*, 1992-1996.

(46) Banks, C. E.; Davies, T. J.; Wildgoose, G. G.; Compton, R. G. Chem. Commun. **2005**, *7*, 829-841.

(47) Banks, C. E.; Moore, R. R.; Davies, T. J.; Compton, R. G. Chem. Commun. **2004**, *16*, 1804-1805.

(48) Banks, C. E.; Compton, R. G. Analyst **2005**, *130*, 123-127.

(49) Huang, Y.; Li, S. F. Y. J. Electroanal. Chem. **2013**, 690, 8-12.

(50) Kaewruksa, B.; Ruangpornvisuti, V. J. Mol. Model. **2012**, *18*, 1447-1454.

(51) Chen, C.; Cai, W.; Long, M.; Zhou, B.; Wu, Y.; Wu, D.; Feng, Y. ACS Nano **2010**, *4*, 6425-6432.

(52) Orzechowska, E.; Kozłowska, E.; Staroń, K.; Trzcińska-Danielewicz, J. Oncol. Rep. **2012**, *27*, 281-285.

(53) Hirpara, J. L.; Clement, M. V.; Pervaiz, S. J. Biol. Chem. **2001**, *276*, 514.

(54) Ahmad, K. A.; Iskandar, K.; Clement, M. V.; Clement, M. V.; Pervaiz, S. Cancer Res. **2004**, *64*, 7867-7878.

(55) Poh, T. W.; Pervaiz, S. Cancer Res. **2005**, *65*, 6264-6274.

(56) Ahmad, K. A.; Wang, G. X.; Ahmed, K. Mol. Cancer Res. **2006**, 4,331-338.

(57) Singh, R. J.; Hogg, N.; Joseph, J.; Kalyanaraman, B. J. Biol. Chem. **1996**, *271*, 18596-18603.

(58) Solomon, S. B.; Bellacia, L.; Sweeney, D.; Piknova, B.; Perlegas, A.; Helms, C. C.; Ferreyra, G. A.; King, S. B. N.; Raat, J. H.; Kern, S. J.; Sun, J.; McPhail, L. C.; Schechter, A. N.; Natanson, C.; Gladwin, M. T.; Kim-Shapiro, D. B. Free Radical Biol. Med. **2012**, *53*, 2229-2239.

Journal of Materials Chemistry B Accepted Manuscript

Table of Contents

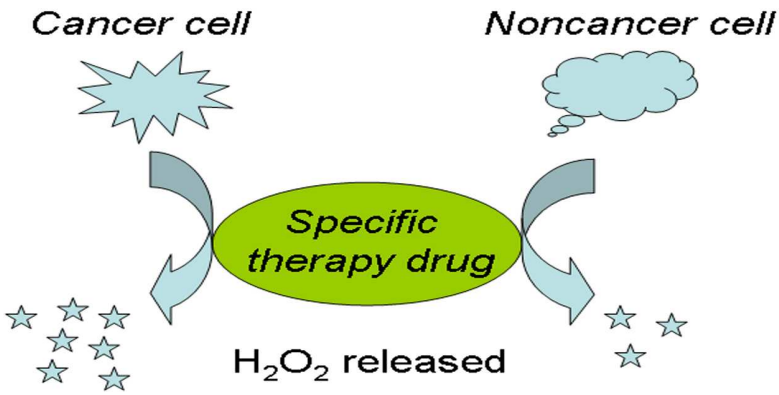

rGO Quantum Dot/ZnO hybrid nanofibers permit a quantitative detection of the H_2O_2 released from cells under the corresponding drugs' stimuli and may be used for drug screening.

Journal of Materials Chemistry B Accepted Manuscript